Ecological Modelling 487 (2024) 110567

Contents lists available at ScienceDirect

Ecological Modelling

journal homepage: www.elsevier.com/locate/ecolmodel

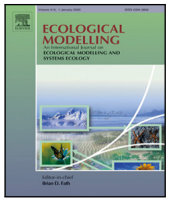

Modelling buoyancy-driven vertical movement of *Trichodesmium* application in the Great Barrier Reef

Chinenye J. Ani [a,b,c,*], Mark Baird [d], Barbara Robson [b,c]

[a] College of Science and Engineering, James Cook University, Townsville, QLD 4811, Australia
[b] Australian Institute of Marine Science, PMB3 Townsville, QLD 4810, Australia
[c] AIMS@JCU, Australian Institute of Marine Science, College of Science and Engineering, James Cook University, Townsville, QLD 4811, Australia
[d] CSIRO Environment, Hobart, Tasmania 7001, Australia

ARTICLE INFO

Dataset link: Trichodesmium-buoyancy (Original data)

Keywords:
Trichodesmium
Buoyancy
Sinking velocity
eReefs
Great Barrier Reef

ABSTRACT

Trichodesmium cells aggregate and form single trichomes or larger colonies and possess strong intracellular gas vesicles that generate strong positive buoyancy and facilitate the vertical migration of colonies. *Trichodesmium* is proposed to be an important source of nitrogen in the Great Barrier Reef (GBR) with implications for nutrient cycling and eutrophication. To understand the dynamics of *Trichodesmium* in the GBR ecosystem, reliable model predictions of *Trichodesmium* growth, nitrogen fixation and distribution are required. The sinking rates of *Trichodesmium* colonies have been reported to be dependent on the shape and size of colonies, and the orientation of colonies in seawater. Therefore, to better simulate the vertical movement of *Trichodesmium* in the GBR, and subsequent biogeochemical dynamics, the *Trichodesmium* processes in the eReefs biogeochemical model was modified by applying the form resistance factor to the sinking velocities of tuft-shaped *Trichodesmium* colonies. Our model results compare well with observations from the Australian Institute of Marine Science Marine Monitoring Program sensor network sites and capture the emergent patterns of phytoplankton size spectrum observed in nature. The modified model formulations improve the physiological realism of the *Trichodesmium* growth submodel of the eReefs marine biogeochemical models, and can help to improve the understanding of *Trichodesmium* dynamics for effective GBR water quality management.

1. Introduction

Trichodesmium is a unique diazotrophic marine cyanobacterium that is widely spread in tropical and subtropical oceans. *Trichodesmium* cells aggregate and form single trichomes or larger colonies and form extensive surface blooms when conditions are favourable (Capone et al., 1997). *Trichodesmium* colony morphology include puff colony, tuft colony, raft colony and bowtie colony (Janson et al., 1995; Hynes et al., 2012). One important characteristic of *Trichodesmium* is its ability to regulate the vertical movement of its colonies in the water column. This process, also known as buoyancy, is facilitated by the strong gas vesicles possessed by *Trichodesmium* (Walsby, 1978; Heimann and Cirés, 2015). These gas vesicles allow *Trichodesmium* to survive in poor nutrient conditions. Other colony forming cyanobacteria such as *Microcystis* also utilise intracellular gas vesicles for buoyancy (Yu et al., 2018; Wei et al., 2021; Li et al., 2022). Additionally, bloom-forming diatoms such as *Thalassiosira* enhance photosynthesis via a robust carbon concentrating mechanism (CCM) or C4-like pathway (Clement et al., 2017; Qiu et al., 2022) and *Phaecocystis* have been assumed to develop a defensive mechanism against predators by increasing its colony size (Kuhlisch et al., 2020; Ryderheim et al., 2022).

In the euphotic zone, *Trichodesmium* fixes and stores carbon and nitrogen (Romans et al., 1994; Held et al., 2022), sinks with this carbon ballast into deep waters where phosphorus can be assimilated (Villareal and Carpenter, 2003; Hewson et al., 2009). *Trichodesmium* gas vesicles are adapted to withstand high pressure experienced in deep waters so that turgor pressure collapse of gas vesicles does not occur (Walsby, 1978). In deep waters, the carbon ballast is metabolised and since gas vesicles are not collapsed, lighter *Trichodesmium* colonies are able to regain buoyancy and float back to surface waters. This enables them to spend more time in the euphotic zone while optimising its access to light and nutrients and may outcompete other phytoplankton species for light and nutrients needed for growth (Huisman et al., 2018). This agrees with Wu et al.'s (2023) suggestion that *Phaecocystis* colony formation provides a competitive advantage over other phytoplankton species for nutrients and light. Thus, *Trichodesmium* buoyancy allows *Trichodesmium* to occur in conditions of varying irradiance and nutrient availability common in tropical and subtropical oceans.

* Corresponding author at: College of Science and Engineering, James Cook University, Townsville, QLD 4811, Australia.
E-mail address: chinenye.ani@my.jcu.edu.au (C.J. Ani).

https://doi.org/10.1016/j.ecolmodel.2023.110567
Received 10 August 2023; Received in revised form 25 September 2023; Accepted 13 November 2023
Available online 18 November 2023

The sinking rates of *Trichodesmium* colonies depend on the shape and size of colonies (Walsby, 1992). Reynolds and Walsby (1975) suggest that larger colonies may sink to greater depth than small colonies due to high sinking velocities. However, Kromkamp and Walsby (1992) reported that larger colonies did not migrate to greater depth: rather they sank faster and the number of colonies that migrated vertically increased. Previous studies on the buoyancy regulation of freshwater diazotrophic *Microcystis* colonies suggest a weak relationship between the size and sinking velocity of colonies when there is increased colony size (Den Uyl et al., 2021) and that variations in *Microcystis* buoyancy could be influenced by irradiance through colony morphology especially under high irradiance (Xu et al., 2023).

Trichodesmium buoyancy varies as a function of the varying balance between gas vesicles and carbohydrate ballast due to changing light conditions, nutrients and other environmental conditions (Kromkamp and Walsby, 1992; Oliver, 1994) or by consuming carbohydrate ballast through the supply of energy to nitrogenase for nitrogen fixation (Held et al., 2022). *Trichodesmium* colonies become more buoyant in low light conditions (because they consume intracellular carbon stores to fuel respiration) and gradually lose their buoyancy in high light (because photosynthesis increases carbon stores) (Walsby, 1969). This is consistent with a previous study on the vertical movement of *Microcystis* colonies as high irradiance reduced buoyancy (Den Uyl et al., 2021). Toxin producing *Nodularia spumigena* have been reported to experience decreased buoyancy in high salinity conditions with implications for the uptake and distribution of nodularian in benthic communities (Carlsson and Rita, 2019).

Surface *Trichodesmium* bloom is formed as a result of the occurrence of buoyancy in very calm conditions (Capone et al., 1997). At the surface *Trichodesmium* photosynthesise and shade out other phytoplankton species, and experience increased mortality due to UV exposure and spread of viral phages through the population. This agrees with Yu et al.'s (2018) suggestion that the vertical distributions of freshwater cyanobacteria influence their competition for light as highly buoyant *Microcystis* outcompete less buoyant *Chlorella* in conditions of low turbulence, high nutrient concentrations and suitable temperatures. Thus, the persistence of *Trichodesmium* in surface waters demonstrates that *Trichodesmium* is not able to perfectly regulate buoyancy. *Trichodesmium* buoyancy variations can impact marine ecosystems as they can facilitate optimal utilisation of light while preventing cell damage due to high irradiance (Subramaniam et al., 1999; Ueno et al., 2016). Buoyancy variations also influence *Trichodesmium* dispersal and distribution in sea waters (Capone et al., 1997; Heimann and Cirés, 2015).

Trichodesmium is proposed to be an important source of nitrogen in the Great Barrier Reef (GBR) — the world's largest coral reef system — with implications for nutrient cycling and eutrophication (Bell, 2021; Ani et al., 2023). Effective GBR water quality management requires an understanding of the contribution of *Trichodesmium* to the total annual nitrogen budget of the GBR. Satellite ocean-colour data (Bell, 2021) and the eReefs models (coupled hydrodynamic-biogeochemical model Baird et al., 2020) (Ani et al., 2023), have been used to estimate the annual contribution of *Trichodesmium* fixed nitrogen to the nitrogen budget of the GBR. Both approaches suggested that the nitrogen fixed by *Trichodesmium* was greater than riverine nitrogen loads exported to the GBR. Therefore, an understanding of the variations in*Trichodesmium* buoyancy is important to improve the understanding of *Trichodesmium* dynamics in GBR ecosystems.

In this study, the influence of *Trichodesmium* colony shape and orientation in seawater on *Trichodesmium* buoyancy was parameterised in the *Trichodesmium* growth submodel of the eReefs biogeochemical models by applying the form resistance factor to the sinking velocities of tuft-shaped *Trichodesmium* colonies found in the GBR (Bell et al., 2005). This would help to provide reliable model simulations of *Trichodesmium* growth, nitrogen fixation and distribution, which are important for improved understanding of *Trichodesmium* dynamics in GBR ecosystems.

2. Methods

2.1. Trichodesmium *buoyancy*

The sinking velocity of particles is influenced by cell size, shape and density. For a spherical particle, Stokes' law (Stokes, 1850) is applied to the sinking velocity, which is given as

$$\mu = \frac{2gr^2(\rho_c - \rho_w)}{9\eta}, \tag{1}$$

where r is the cell radius, g is gravity, ρ_w is the water density, ρ_c is the cell density and η is the coefficient of the dynamic viscosity of the water. The version of the *Trichodesmium* growth model described by Robson et al. (2013) and Baird et al. (2020) assumes a spherical *Trichodesmium* colony with radius $r = 5$ μm and used (1) to represent *Trichodesmium* sinking velocity. However, *Trichodesmium erythraeum* colonies in the GBR have been reported to be tuft shaped (Bell et al., 2005).

McNown and Malaika (1950) applied the form resistance factor Φ to the sinking velocity of non-spherical cells. The sinking velocity of non-spherical cells with volume V is defined as

$$\mu = \frac{2gr_e^2(\rho_c - \rho_w)}{9\eta\Phi}, \tag{2}$$

where r_e is the effective radius given by

$$r_e = \left(\frac{3V}{4\pi}\right)^{\frac{1}{3}}. \tag{3}$$

The form resistance factor is the factor by which the sinking velocity of a non-spherical particle differs from that of a sphere of equal volume and density. A spherical cell has $\Phi = 1$. At low Reynolds number, symmetrically weighted non-spherical objects remain in their original orientation when sinking and the settling velocity of a cylindrical object is similar to that of an ellipsoid of the same axial ratio, density and volume (McNown and Malaika, 1950).

Here, we represent *Trichodesmium* tufts as ellipsoids. Although in reality, tufts do not have the smooth surface of an ellipsoid, given the small size of the tufts and laminar fluid dynamics involved, this surface roughness will not significantly affect form resistance.

Following Walsby and Holland (2006), the form resistance coefficient of an ellipsoid with semi-axes a, b and c is given as

$$\Phi = \frac{16}{3D(\Psi + \Omega)}, \tag{4}$$

where Ψ is a shape factor independent of orientation, Ω is an orientation-dependent shape factor relative to the direction of movement, and $D = 2(abc)^{\frac{1}{3}}$ is the nominal diameter. The filaments of a cylindrical cell of width w and length l have volume

$$V = \pi\left(\frac{w}{2}\right)^2 l \tag{5}$$

and from (3), the effective radius

$$r_e = \left(\frac{3}{16}w^2 l\right)^{\frac{1}{3}}. \tag{6}$$

For a horizontally oriented cell (Fig. 1(a)),

$$a = c < b, b = \frac{l}{2}, a = \frac{w}{2}, \Psi = \Psi_{hor}, \Omega = \Omega_{hor}.$$

A vertically oriented cell (Fig. 1(b)) has

$$a > b = c, a = \frac{l}{2}, b = \frac{w}{2}, \Psi = \Psi_{vert}, \Omega = \Omega_{vert}.$$

See Walsby and Holland (2006) for detailed derivations of Ψ_{vert}, Ψ_{hor}, Ω_{vert} and Ω_{hor}. The form resistance coefficient and effective radius of a tuft-shaped *Trichodesmium erythraeum* colony with length 1000–2000 μm and width (diameter) 50–150 μm (Post et al., 2002) are calculated using (4) where

$$\Psi = \frac{\Psi_{vert} + \Psi_{hor}}{2} \tag{7}$$

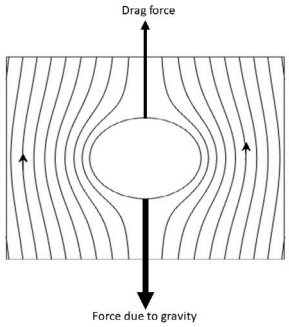

(a) Horizontally oriented sinking ellipsoid.

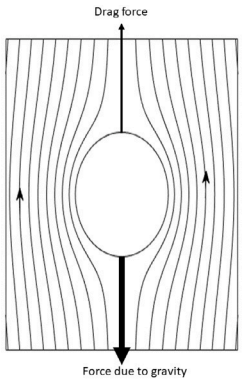

(b) Vertically oriented sinking ellipsoid.

Fig. 1. Theoretical streamlines for flow around a sinking ellipsoid. The thickness of the force arrows indicates the magnitude of the forces. For example, relative to the horizontally oriented sinking ellipsoid, the magnitude of the drag force reduced when the sinking ellipsoid is vertically oriented whereas the force due to gravity remained constant and is greater than the drag force in both scenarios.

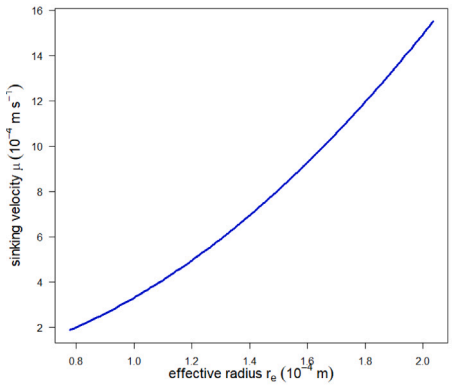

(a) Sinking velocity versus effective radius.

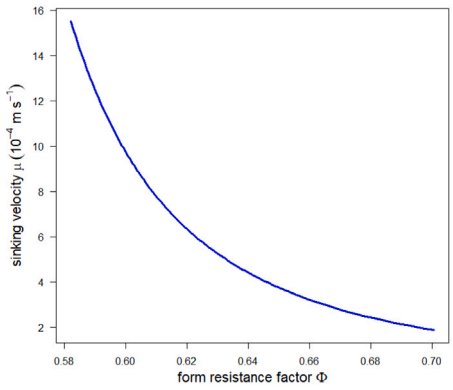

(b) Sinking velocity versus form resistance factor.

Fig. 2. Relationships between the sinking velocity (2) and the effective radius (3), the sinking velocity and the form resistance factor (4) of a tuft-shaped *Trichodesmium* colony of length 1000–2000 μm and width (diameter) 50–150 μm (Post et al., 2002).

and

$$\Omega = \frac{\Omega_{vert} + \Omega_{hor}}{2}. \tag{8}$$

Using (2) the buoyancy regulation of *Trichodesmium* in the water column is represented by the model as

$$\frac{\partial Tricho}{\partial t} = -\frac{2gr_e^2(\rho_c - \rho_w)}{9\eta\Phi}\frac{\partial Tricho}{\partial z}, \tag{9}$$

where

$$\rho_c = \rho_{min} + R_C^*(\rho_{max} - \rho_{min}), \tag{10}$$

z is the distance in the vertical. The parameters ρ_{min} and ρ_{max} constrain the calculation of *Trichodesmium* colony density and R_C^* represents carbon reserves. These modified formulations increase the sinking rate of a *Trichodesmium* colony in the model and are in the range −0.8 to 0.8 mm s^{-1} reported by Walsby (1978). Fig. 2 shows the relationship between the sinking velocity, the effective radius and the form resistance factor of a tuft-shaped *Trichodesmium* colony in the model. Detailed descriptions of the EMS *Trichodesmium* growth model are available in Robson et al. (2013) and Baird et al. (2020) (see Table 1 for constants and parameters for the *Trichodesmium* growth model).

2.2. Model forcing

The eReefs hydrodynamic model was forced with outputs from the 10 km Ocean Modelling Analysis and Prediction System (OceanMAPS – https://researchdata.edu.au/oceanmaps-analysis/1440629), the 12 km Australian Community Climate and Earth-System Simulator (ACCESS-R – http://www.bom.gov.au/nwp/doc/access/NWPData.shtml) and river flow data from 22 rivers. The biogeochemical model was forced with simulated hydrodynamic model outputs, wave data from the Bureau of Meteorology (BoM) regional wave model AUSWAVE-R and P2R GBR Dynamic SedNet with 2019 catchment conditions of nutrient and sediment loads (McCloskey et al., 2017, 2021a,b). The eReefs hydrodynamic model (version 2.0) configured at 4 km resolutions (GBR4 grid) with the modified sinking velocity and the *Trichodesmium* growth model in Ani et al. (2023) was run from December 1, 2010 to November 30, 2012. The modified model is denoted as GBR4-BGC-cyl.

2.3. Model evaluation

Fourteen observation sites from the Australian Institute of Marine Science (AIMS) Marine Monitoring Program (MMP) sensor network sites (Australian Institute of Marine Science (AIMS), 2023) (Fig. 3) sampled tri-annually and time series of simulated model outputs from version 3.2 of the biogeochemical model of the eReefs model described in Baird et al. (2020) (hereafter referred to as GBR4-BGC-sph) were used to evaluate the modified model. Observations obtained from the fourteen monitoring sites were available throughout the period of model simulation (See Skerratt et al. (2019) for more information on AIMS MMP sites).

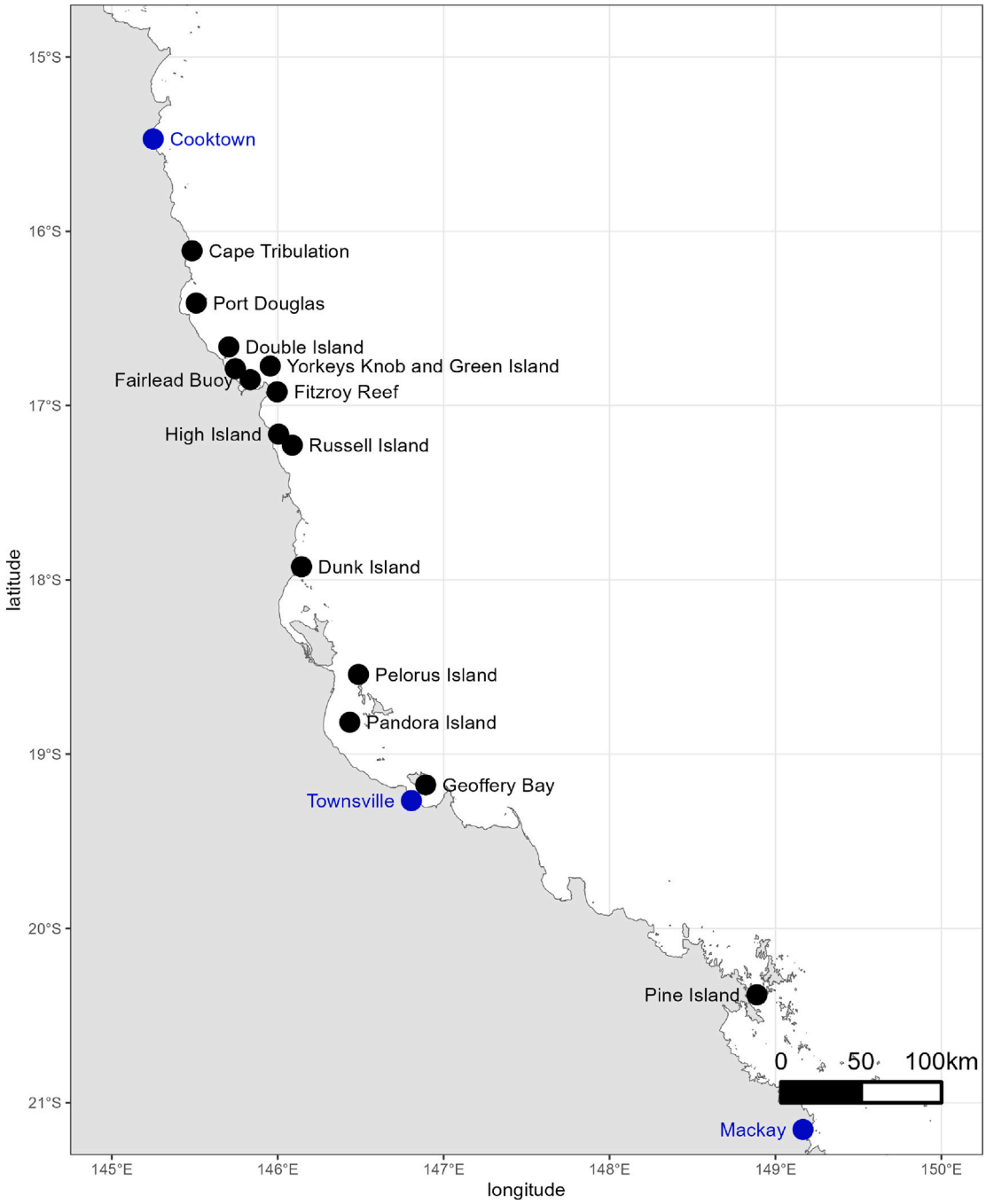

Fig. 3. Sample sites: the Australian Institute of Marine Science (AIMS) Marine Monitoring Program (MMP) sensor locations (black symbol) and towns (blue symbol).

Table 1
Constants and parameters for the *Trichodesmium* growth model.

Variable	Symbol	Units	Reference
Constants			
Acceleration due to gravity	g	9.81 m s^{-2}	–
Dynamic viscosity of water at 20 °C	μ	0.001 Pa s	–
Parameters			
Trichodesmium cell radius	r	5 μm	Robson et al. (2013)
Trichodesmium colony effective radius	r_e	140 μm	–
Trichodesmium form resistance factor	Φ	0.61	–
Minimum cell density	ρ_{min}	1010 kg m^{-3}	Calculated from observed maximum rising rates in Walsby (1978)
Maximum cell density	ρ_{max}	1030 kg m^{-3}	Calculated from observed maximum sinking rates in Walsby (1978)

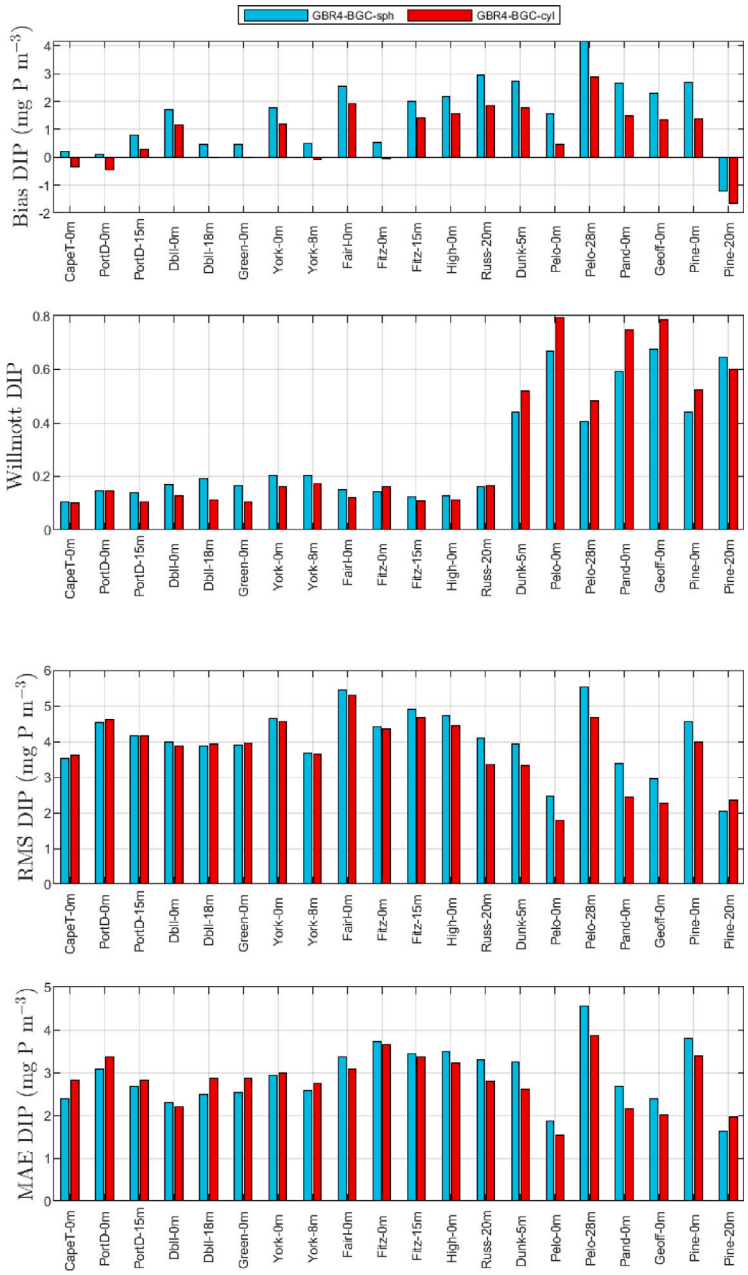

Fig. 4. From top to bottom: bias, Willmott score, root mean square error and mean absolute error for simulated dissolved inorganic phosphorus (DIP) versus monthly observations from December 2010 to November 2012 (Moran et al., 2022). Sites are arranged from North to South and locations are shown in Fig. 3. Water quality sampling was done at more than one depth at some sites. The *x*-axis labels represent the short form of the station name followed by the depth in metres below the surface. Index of short names to full station names: CapeT = "Cape Tribulation"; PortD = "Port Douglas"; DblI = "Double Island"; Green = "Green Island"; York = "Yorkeys Knob"; Fairl = "Fairlead Buoy"; Fitz = "Fitzroy Reef"; High = "High Island"; Russ = "Russell Island"; Dunk = "Dunk Island"; Pelo = "Pelorus Island"; Pand = "Pandora Island"; Geoff = "Geoffery Bay"; Pine = "Pine Island". "GBR4-BGC-sph" corresponds to the version of the model described in Baird et al. (2020) whereas "GBR4-BGC-cyl" is the modified model.

The variables considered for validation include chlorophyll-*a* (Chl-*a*) extractions, dissolved inorganic phosphorus (DIP), ammonium (NH_4) and nitrate + nitrite [NO_x]. The skill metrics used to validate the modified model include, bias, Willmott score, root mean square error (RMS) and mean absolute error (MAE). Bias examines the model's over- or under-prediction of observations. The Willmott score varies between 0 and 1 and is a ratio of the mean square error and the mean absolute deviation about the observed mean (Willmott et al., 1985). A Willmott score of 1 indicates a perfect match and 0 indicates no match. For this study, following Skerratt et al. (2019) and Robson et al. (2020), a Willmott score of 0.6 against simulated water quality variables was used as a benchmark for excellent model fit. RMS measures model accuracy, i.e., the difference between model predictions and observations. An RMS of 0 indicates perfect fit.

The emergent properties of phytoplankton community structure were assessed using 15,000 randomly sampled simulated surface data points from December 2010 to November 2012. The variation of the percentage of Chl-*a* contained in large phytoplankton (including *Trichodesmium*) and small phytoplankton as a function of chlorophyll were examined. These relationships were compared with observed relationships reported by Brewin et al. (2010) and Hirata et al. (2011) from analyses on a global marine phytoplankton database. Additionally, the relationship between simulated zooplankton biomass and Chl-*a* were

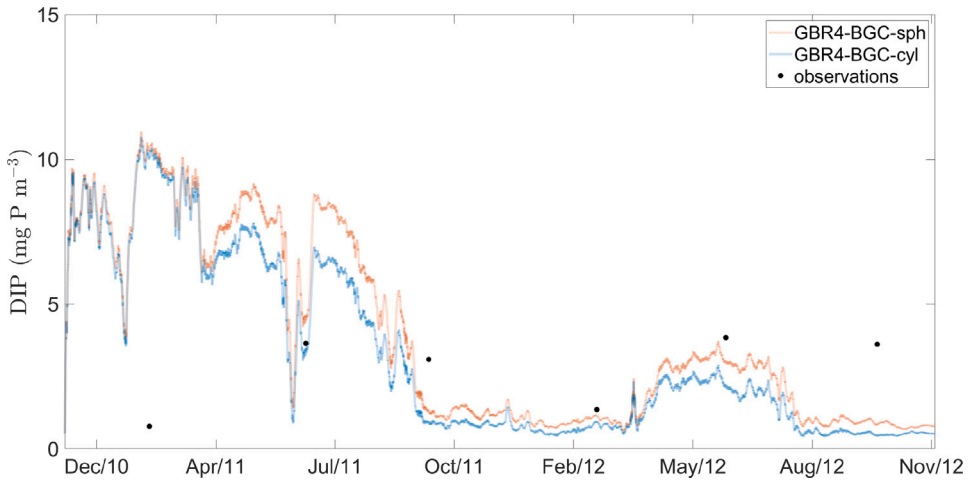

Fig. 5. Comparison of the time series of simulated and observed DIP concentrations at 15 m Port Douglas. GBR4-BGC (orange), modified GBR4-BGC (blue) and observations (black).

compared with that of GBR4-BGC-sph using 15,000 randomly sampled surface data points.

3. Results

3.1. Skill assessment

The comparison of simulated GBR4-BGC-sph DIP and DIP observations from the MMP sites had an average Willmott index of 0.29 and bias 1.16 mg P m^{-3} (Fig. 4). Simulated DIP from the modified GBR4-BGC-cyl had a higher mean Willmott index (0.30) and a higher bias (1.31 mg P m^{-3}). DIP concentrations were overestimated by both models.

Simulated GBR4-BGC-sph Chl-*a* extractions and observations of Chl-*a* extractions had an average Willmott index of 0.47 and mean bias of 0.12 mg Chl-*a* m^{-3} (Supplementary Information — Figure **S1**). Chl-*a* extractions from samples at MMP sites and simulated Chl-*a* extractions from GBR4-BGC-cyl had a lower average Willmott index (0.43) and higher bias of 0.18 mg Chl-*a* m^{-3} when compared to the GBR4-BGC-sph Chl-*a* extractions at the same sites. Both models overestimate Chl-*a* extractions at all sites except at Yorkey's knob, Dunk Island Pandora Island which are in waters very close to the mainland and are surrounded by shallow and muddy seabed.

Figure **S2** (Supplementary Information) shows that the comparison of simulated GBR4-BGC-sph NH_4 and NH_4 observations had an average bias of −0.36 mg N m^{-3} and Willmott index of 0.39. Simulated NH_4 from the modified model had a lower average Willmott index (0.37) and mean bias −0.36 mg N m^{-3}. Both GBR4-BGC-sph and GBR4-BGC-cyl underestimate NH_4 at all the sites expect at Fitzroy Reef and Pelorus Island.

Simulated NO_3 from GBR4-BGC-sph and GBR4-BGC-cyl were compared with tri-annually sampled NO_3 and had an average Willmott index of 0.25 and −0.07 mg N m^{-3} bias (Supplementary Information — Figure **S3**). On the other hand, simulated NO_3 from GBR4-BGC-cyl model had a mean Willmott index (0.25) and lower mean bias (−0.19 mg N m^{-3}). NO_3 was underestimated by both models at 65% of the MMP sites.

The model simulations capture the impacts of record high rainfall experienced in north and eastern Australia during the 2010/2011 wet season (from December to February — caused by peak La Niña conditions) as simulated DIP, NH_4 and NO_3 concentrations, and Chl-*a* extractions during the 2010/2011 wet season were higher when compared with the 2011/2012 wet season (Fig. 5 and Figure **S4** — Supplementary Information).

The representation of nitrogen and phosphorus cycles in the model is complex, so the systematic overestimation of DIP and (at some sites) underestimation of Chl-*a* could have a range of possible causes. For example, the models' overestimation of DIP could reflect an underestimation of the adsorption of phosphorus to sediment particle surfaces due to an error in the parameter controlling adsorption–desorption, or an error in the net balance between phytoplankton uptake and mortality (or grazing) and subsequent remineralisation of organic matter, or an error in the parameters defining sediment remineralisation rates, or from an underestimation of uptake by benthic organisms. Similarly, the underestimation of NH_4 and NO_3 at most sites could be from an error in the net balance between phytoplankton uptake and mortality (or grazing) and subsequent remineralisation of organic matter in the water column, or an overestimation of uptake by benthic biota, or in the balance between nitrification, denitrification and anaerobic ammonium oxidation rates, and nitrogen fixation rates. The conceptual diagrams summarising the nitrogen and phosphorus fluxes in the eReefs model can be found in the Supplementary Information (Figures **S5** and **S6**).

3.2. Emergent relationships and trichodesmium dynamics

Emergent relationships are system-level patterns observed in nature that occur as ecosystem functions and are used as indicators to assess that models accurately capture important biogeochemical processes especially when there are limited observations for model assessment (Robson et al., 2017; Hipsey et al., 2020; Robson et al., 2020). Emergent relationship between the percentage of small vs large phytoplankton and chlorophyll *a* in global ocean data sets (Brewin et al., 2010; Hirata et al., 2011) was used by Robson et al. (2017, 2020) to provide an additional layer for the assessment of the eReefs marine models.

Fig. 6 shows the relationship between small and large phytoplankton and total chlorophyll from GBR4-BGC-sph, GBR4-BGC-cyl and observations. GBR4-BGC-cyl better captures the emergent patterns observed in nature. This increases our confidence that the model is correctly simulating the processes that underlie competition and coexistence of phytoplankton of different size classes. Fig. 7 shows that both models are similar with respect to their ability to reproduce the expected emergent relationship between zooplankton concentrations and chlorophyll *a* concentrations.

The difference between mean surface *Trichodesmium* concentrations from GBR4-BGC-cyl and GBR4-BGC-sph during summer is shown in Fig. 8. GBR4-BGC-cyl *Trichodesium* concentrations are slightly higher than that of GBR4-BGC-sph in the southern GBR cross-shelf waters, lower in central and northern cross-shelf waters and northern GBR

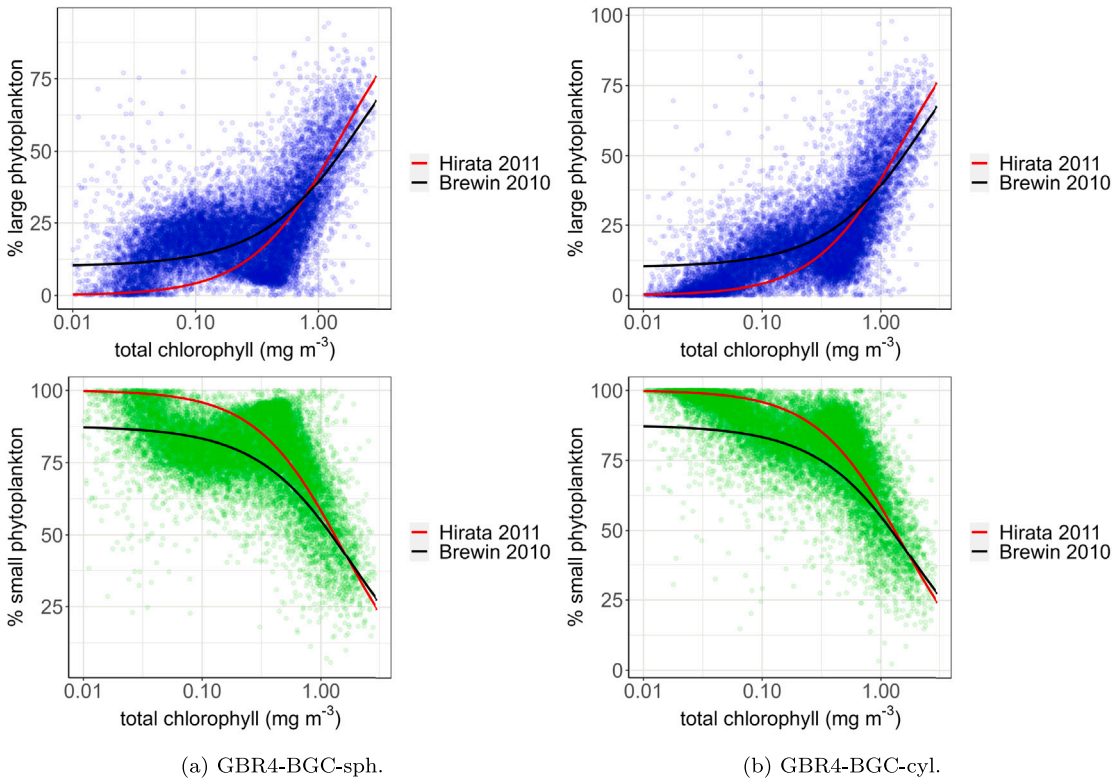

Fig. 6. Relationship between the percentage of randomly sampled simulated surface large phytoplankton and chlorophyll *a* concentrations (top), simulated surface small phytoplankton and chlorophyll *a* concentrations (bottom). Dots represent randomly sampled simulated data points and lines show fits to observations from a global marine database taken from Hirata et al. (2011). Large phytoplankton comprises microphytoplankton and *Trichodesium* and small phytoplankton consists of nano- and pico-phytoplankton.

domain, and are similar to GBR4-BGC-sph *Trichodesium* concentrations in other parts of the GBR domain.

The modified model simulates the vertical distribution of *Trichodesmium*. Intracellular *Trichodesmium* total nitrogen are highest at the surface (Fig. 9(a)) but intracellular *Trichodesmium* chlorophyll *a* concentrations are higher at intermediate depths (Fig. 9(b)). Intracellular *Trichodesmium* carbon reserves and nitrogen fixation rates are lowest in deep and dark conditions (Figs. 9(c) and 9(d)).

4. Discussion

4.1. The impacts of variations in buoyancy on trichodesmium distribution in the GBR

The vertical distribution of *Trichodesmium* dynamics is influenced by variations in buoyancy. The interactions between variations in buoyancy and changing environmental conditions such as light, temperature and nutrient availability can alter the occurrence of *Trichodesmium* and other marine organisms. In calm, temperature-suitable and nutrient-rich conditions, *Trichodesmium* blooms, dominates the surface layer and shades out other phytoplankton species. On the contrary, in calm and stratified waters diatoms and green algae sink beneath the stratified layer where light intensity is low and zooplankton grazing is high due to their small sizes (Yu et al., 2018). These processes allow *Trichodesmium* to outcompete other phytoplankton species for light and nutrients required for growth. However, increased sinking of *Trichodesmium* colonies can increase the growth of other phytoplankton species due to increased influx of light and nutrient availability for other phytoplankton growth (Benavides et al., 2022).

Variations in buoyancy allow *Trichodesmium* colonies to overcome the inhibiting effect of low phosphorus concentration on growth in oligotrophic waters by migrating to deeper waters to assimilate both inorganic and organic phosphorus (Beversdorf et al., 2010; White et al., 2010). Thus, the reduced DIP concentrations from the modified GBR4-BGC-cyl at 15 m below the sea surface shown in Fig. 5 could be due to increased phosphorus uptake by fast-sinking *Trichodesmium* colonies.

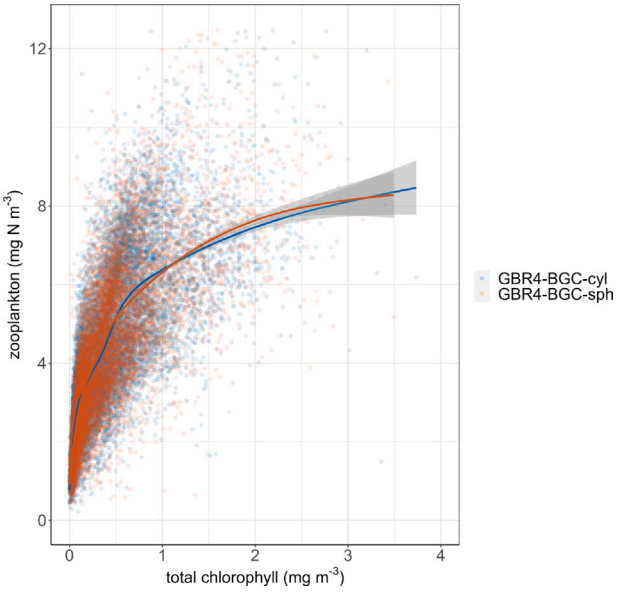

Fig. 7. Relationship between 15,000 randomly sampled simulated surface zooplankton and chlorophyll *a* concentrations. The smoothing functions applied to the data are represented by lines and grey-shaded confidence intervals.

Trichodesmium colonies mostly photosynthesise and fix nitrogen at the surface under high irradiance. Decreased mean surface GBR4-BGC-cyl *Trichodesmium* concentrations during summer (wet season) shown

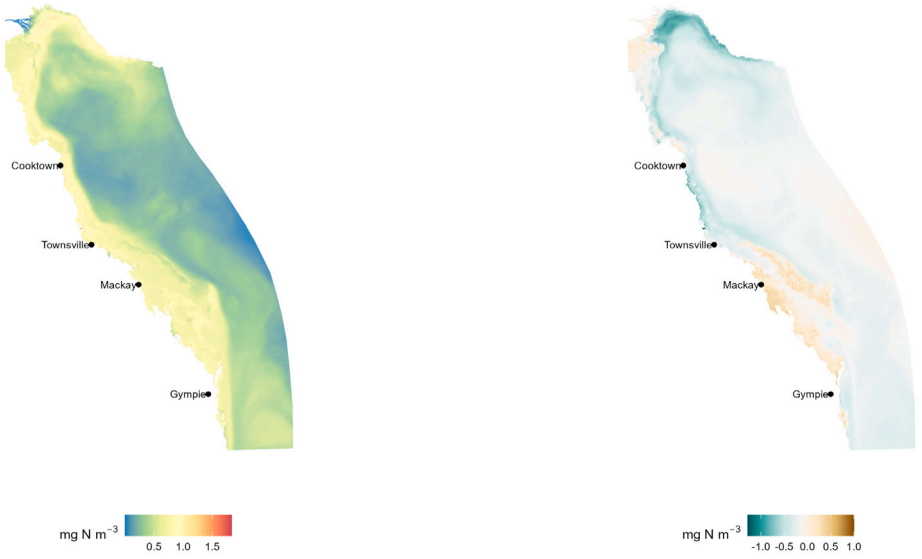

(a) GBR4-BGC-sph (b) GBR4-BGC-cyl − GBR4-BGC-sph

Fig. 8. Spatially-resolved GBR4-BGC-sph mean surface *Trichodesmium* concentrations (Fig. 8(a)), and the difference between GBR4-BGC-cyl and GBR4-BGC-sph mean surface *Trichodesmium* concentrations (Fig. 8(b)) during summer (from 2 December 2010 to 1 March 2011) in the Great Barrier Reef.

in most parts of the GBR cross-shelf waters and northern GBR domain (Fig. 8) is likely due to increased number of sinking *Trichodesmium* colonies, which sink faster to deep waters where reduced carbon and nitrogen fixation occur (Benavides et al., 2022; Ani et al., 2023). This agrees with Kromkamp and Walsby's (1992) report that large *Trichodesmium* colonies sink faster and the number of colonies that migrate vertically increased. However, increased mean surface GBR4-BGC-cyl *Trichodesmium* concentrations shown in southern cross-shelf waters could be as a result of increased number of trapped colonies due to the inadequacy of *Trichodesmium* to perfectly regulate buoyancy and the effects of high DIP concentrations from river discharge on *Trichodesmium* growth.

4.2. The impacts of variations in buoyancy on trichodesmium physiology

The decrease in simulated *Trichodesmium* total nitrogen with depth (Fig. 9(a)) is likely influenced by the inhibiting effects of low irradiance on *Trichodesmium* growth. However, *Trichodesmium* chlorophyll *a* concentrations are higher at intermediate depths (Fig. 9(b)) because the model's production of chlorophyll is stimulated in low light conditions when sufficient intracellular carbon, nitrogen and phosphorus are available. The model results suggest that the dynamics of *Trichodesmium* nitrogen and chlorophyll stores may be quite different and cannot be assumed to covary.

Trichodesmium colonies in deep waters will continue to fix nitrogen, but at a reduced rate because nitrogen fixation is inhibited by high DIN concentrations (Benavides et al., 2022; Ani et al., 2023). This is supported by the reduced *Trichodesmium* nitrogen fixation rate in deep waters shown in Fig. 9(d). Below the euphotic zone, *Trichodesmium* uses carbon stores acquired before sinking to fix nitrogen and can also obtain carbon from dissolved organic matter. This can reduce *Trichodesmium* growth in deep waters and is evident in Fig. 9(a) as the structural *Trichodesmium* nitrogen indicating *Trichodesmium* abundance decreased with depth. Our model results show the reduction of intracellular carbon reserves in deep and dark conditions (Fig. 9(c)). Also, Figs. 9(c) and 9(d) show that nitrogen fixation rate is highest when intracellular carbon reserves are high. This is because of the energetic cost of nitrogen fixation as *Trichodesmium* utilises fixed carbon to fix nitrogen from atmospheric dinitrogen (Oliver et al., 2012). The decrease in temperature in deep waters (which reduces *Trichodesmium* metabolism (Boyd et al., 2013; Ani and Robson, 2021)), increased oxygen saturation at depth and reduced nitrogen fixation reduce the consumption of fixed carbon, thus allowing *Trichodesmium* to survive below the euphotic zone before recovering buoyancy. Moreover, the ability of *Trichodesmium* to occur in lower temperature conditions (White et al., 2006) can allow them survive in deep and dark conditions.

4.3. Model limitations

It is important to note that the model developed here does not consider all phenomena relevant to variations in *Trichodesmium* buoyancy. For example, the model formulations used in this study do not include effects of obliquely oriented colonies on *Trichodesmium* sinking rates or variations in tuft size and shape. Obliquely oriented non-spherical colonies or cells have been shown to drift sideways while sinking thereby enhancing their lateral dispersion (Holland, 2010). In addition, *Trichodesmium* colonies were assumed to be symmetrically weighted. However, all asymmetrically weighted colonies have been reported to sink in one orientation (McNown and Malaika, 1950) and can alter their sinking rates.

5. Conclusions

The model formulations developed in this study improve the physiological realism of the *Trichodesmium* growth submodel of the eReefs marine biogeochemical models, and should therefore improve the accuracy of the model outputs. However, the skill assessment results show that the modified model's skill is similar to that of the version of the model in Baird et al. (2020) and where it is different it is slightly worse, although the modified model better captures the emergent patterns of phytoplankton size spectrum observed in nature, thus increasing our confidence in the model's predictions. Therefore, there is need to validate *Trichodesmium* concentrations or nitrogen fixation rates against observations but at present, very limited observational data are available.

Furthermore, our model findings show that variations in *Trichodesmium* buoyancy influences the vertical distribution of *Trichodesmium* in the GBR and its interaction with changing environmental conditions can modify the occurrence of *Trichodesmium* and other marine organisms in the GBR. Finally, our model results suggest that

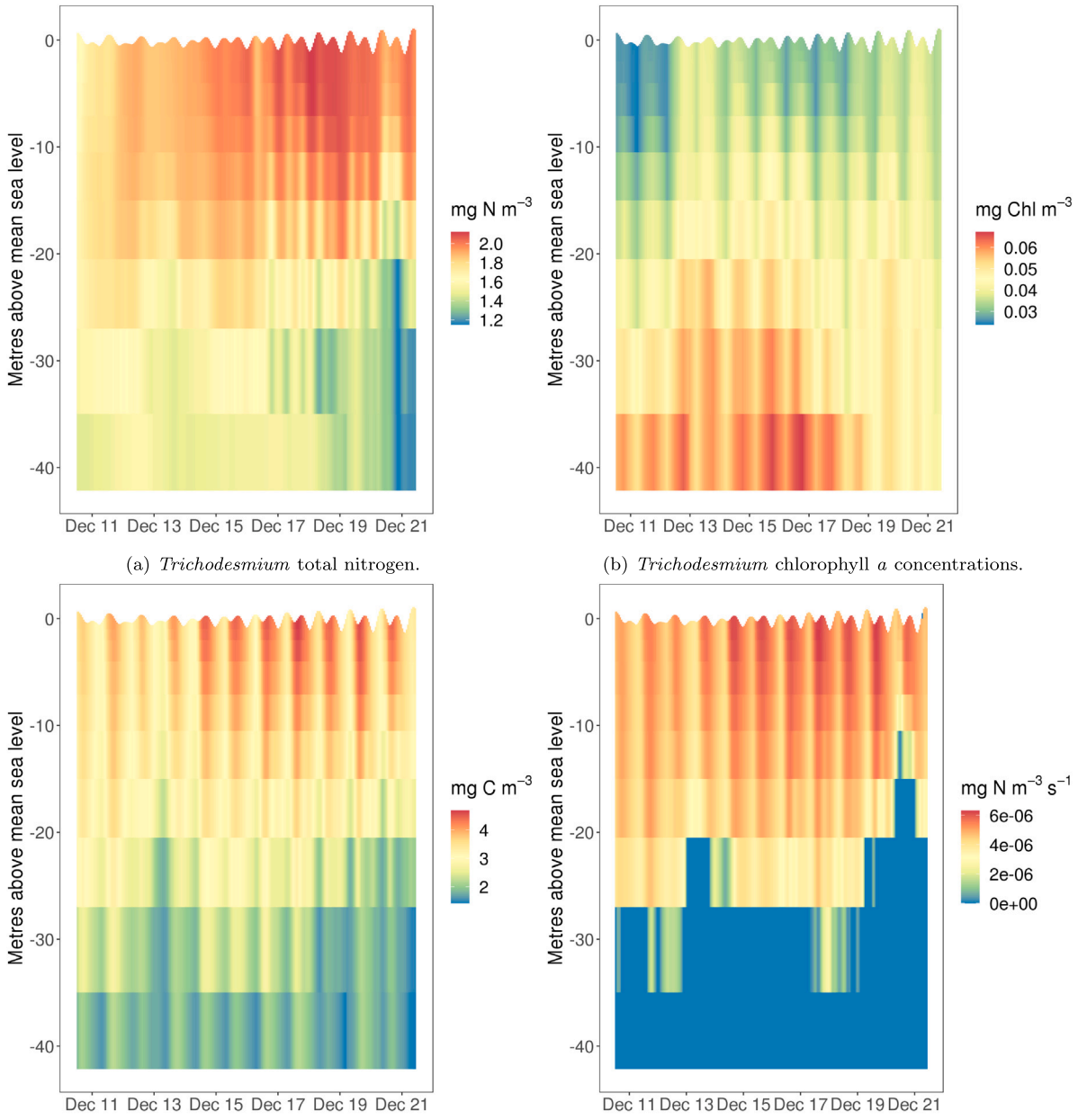

(a) *Trichodesmium* total nitrogen.

(b) *Trichodesmium* chlorophyll *a* concentrations.

(c) *Trichodesmium* carbon reserves.

(d) *Trichodesmium* nitrogen fixation rate.

Fig. 9. Depth profile over time of simulated intracellular *Trichodesmium* nitrogen store (combination of nitrogen and nitrogen reserves), intracellular chlorophyll *a* concentrations, intracellular carbon reserves, and *Trichodesmium* nitrogen fixation rate at the geolocation (17.75°S, 146.6°E) from midday 10/12/2010 to midday 22/12/2010.

observations of the presence or absence of *Trichodesmium* surface blooms are not sufficient to characterise the role of this cyanobacterium in the GBR.

CRediT authorship contribution statement

Chinenye J. Ani: Methodology, Software, Validation, Visualisation, Formal analysis, Investigation, Conceptualization, Resources, Data curation, Writing – original draft. **Mark Baird:** Methodology, Writing – review & editing. **Barbara Robson:** Methodology, Validation, Resources, Writing – review & editing, Supervision, Project administration, Conceptualization, Funding acquisition.

Declaration of competing interest

The authors declare the following financial interests/personal relationships which may be considered as potential competing interests: Chinenye J. Ani reports financial support was provided by James Cook University. Chinenye J. Ani reports financial support was provided by the Australian Institute of Marine Science. Chinenye J. Ani reports financial support was provided by Queensland Water Modelling Network (QWMN).

Data availability

Metadata is available at

Trichodesmium-buoyancy (Original data) (GitHub)

.

Acknowledgements

The Marine Monitoring Program (MMP) managed by the Great Barrier Reef Marine Park Authority provided tri-annually sampled data

available from https://apps.aims.gov.au/metadata/search. Thanks to AIMS@JCU and QWMN for funding this research. Special thanks to Dr Stephen Lewis and A/Prof Scott Smithers for their support as part of the PhD supervision team of Chinenye J. Ani.

Funding information

Funding: this work was supported by AIMS@JCU PhD Scholarship; Queensland Water Modelling Network, a Program of the Queensland Government Department of Environment and Science.

Appendix A. Supplementary data

Supplementary material related to this article can be found online at https://doi.org/10.1016/j.ecolmodel.2023.110567.

References

Ani, C.J., Robson, B., 2021. Responses of marine ecosystems to climate change impacts and their treatment in biogeochemical ecosystem models. Mar. Pollut. Bull. 166, 112223.

Ani, C.J., Smithers, S.G., Lewis, S., Baird, M., Robson, B., 2023. Ereefs modelling suggests *trichodesmium* may be a major nitrogen source in the Great Barrier Reef. Estuar. Coast. Shelf Sci. 108306.

Australian Institute of Marine Science (AIMS), 2023. Great barrier reef marine monitoring program for inshore water quality (MMP WQ). https://apps.aims.gov.au/metadata/view/2b2aa4e4-1368-49e0-8b25-1559ee297854, Accessed 10 December 2020.

Baird, M., Wild-Allen, K., Parslow, J., Mongin, M., Robson, B., Skerratt, J., Rizwi, F., Soja-Wozniak, M., Jones, E., Herzfeld, M., et al., 2020. CSIRO environmental modelling suite (EMS): scientific description of the optical and biogeochemical models (vB3p0). Geosci. Model Dev. 13, 4503–4553.

Bell, P.R., 2021. Analysis of satellite imagery using a simple algorithm supports evidence that *trichodesmium* supplies a significant new nitrogen load to the GBR lagoon. Ambio 50 (6), 1200–1210.

Bell, P.R., Uwins, P.J., Elmetri, I., Phillips, J.A., Fu, F.-X., Yago, A.J., 2005. Laboratory culture studies of *trichodesmium* isolated from the Great Barrier Reef Lagoon, Australia. Hydrobiologia 532, 9–21.

Benavides, M., Bonnet, S., Le Moigne, F.A., Armin, G., Inomura, K., Hallstrø m, S.r., Riemann, L., Berman-Frank, I., Poletti, E., Garel, M., et al., 2022. Sinking *trichodesmium* fixes nitrogen in the dark ocean. ISME J. 1–8.

Beversdorf, L., White, A., Björkman, K., Letelier, R., Karl, D., 2010. Phosphonate metabolism by *trichodesmium* IMS101 and the production of greenhouse gases. Limnol. oceanogr. 55 (4), 1768–1778.

Boyd, P.W., Rynearson, T.A., Armstrong, E.A., Fu, F., Hayashi, K., Hu, Z., Hutchins, D.A., Kudela, R.M., Litchman, E., Mulholland, M.R., et al., 2013. Marine phytoplankton temperature versus growth responses from polar to tropical waters–outcome of a scientific community-wide study. PLoS One 8 (5), e63091.

Brewin, R.J., Sathyendranath, S., Hirata, T., Lavender, S.J., Barciela, R.M., Hardman-Mountford, N.J., 2010. A three-component model of phytoplankton size class for the Atlantic Ocean. Ecol. Model. 221 (11), 1472–1483.

Capone, D.G., Zehr, J.P., Paerl, H.W., Bergman, B., Carpenter, E.J., 1997. *Trichodesmium*, a globally significant marine cyanobacterium. Science 276 (5316), 1221–1229.

Carlsson, P., Rita, D., 2019. Sedimentation of *nodularia spumigena* and distribution of nodularin in the food web during transport of a cyanobacterial bloom from the Baltic Sea to the Kattegat. Harmful Algae 86, 74–83.

Clement, R., Jensen, E., Prioretti, L., Maberly, S.C., Gontero, B., 2017. Diversity of CO_2-concentrating mechanisms and responses to CO_2 concentration in marine and freshwater diatoms. J. Exp. Bot. 68 (14), 3925–3935.

Den Uyl, P.A., Harrison, S.B., Godwin, C.M., Rowe, M.D., Strickler, J.R., Vanderploeg, H.A., 2021. Comparative analysis of *microcystis* buoyancy in western Lake Erie and Saginaw Bay of Lake Huron. Harmful Algae 108, 102102.

Heimann, K., Cirés, S., 2015. N_2-fixing cyanobacteria: ecology and biotechnological applications. In: Handbook of Marine Microalgae. Elsevier, pp. 501–515.

Held, N.A., Waterbury, J.B., Webb, E.A., Kellogg, R.M., McIlvin, M.R., Jakuba, M., Valois, F.W., Moran, D.M., Sutherland, K.M., Saito, M.A., 2022. Dynamic diel proteome and daytime nitrogenase activity supports buoyancy in the cyanobacterium *trichodesmium*. Nat. Microbiol. 7 (2), 300–311.

Hewson, I., Poretsky, R.S., Dyhrman, S.T., Zielinski, B., White, A.E., Tripp, H.J., Montoya, J.P., Zehr, J.P., 2009. Microbial community gene expression within colonies of the diazotroph, *trichodesmium*, from the Southwest Pacific Ocean. ISME J. 3 (11), 1286–1300.

Hipsey, M.R., Gal, G., Arhonditsis, G.B., Carey, C.C., Elliott, J.A., Frassl, M.A., Janse, J.H., de Mora, L., Robson, B.J., 2020. A system of metrics for the assessment and improvement of aquatic ecosystem models. Environ. Model. Softw. 128, 104697.

Hirata, T., Hardman-Mountford, N., Brewin, R., Aiken, J., Barlow, R., Suzuki, K., Isada, T., Howell, E., Hashioka, T., Noguchi-Aita, M., et al., 2011. Synoptic relationships between surface Chlorophyll-a and diagnostic pigments specific to phytoplankton functional types. Biogeosciences 8 (2), 311–327.

Holland, D.P., 2010. Sinking rates of phytoplankton filaments orientated at different angles: theory and physical model. J. Plankton Res. 32 (9), 1327–1336.

Huisman, J., Codd, G.A., Paerl, H.W., Ibelings, B.W., Verspagen, J.M., Visser, P.M., 2018. Cyanobacterial blooms. Nat. Rev. Microbiol. 16 (8), 471–483.

Hynes, A.M., Webb, E.A., Doney, S.C., Waterbury, J.B., 2012. Comparison of cultured *trichodesmium* (cyanophyceae) with species characterized from the field 1. J. Phycol. 48 (1), 196–210.

Janson, S., Siddiqui, P.J., Walsby, A.E., Romans, K.M., Carpenter, E.J., Bergman, B., 1995. Cytomorphological characterization of the planktonic diazotrophic cyanobacteria *trichodesmium spp.* from the Indian ocean and Caribbean and Sargasso Seas 1. J. Phycology 31 (3), 463–477.

Kromkamp, J., Walsby, A.E., 1992. Buoyancy regulation and vertical migration of *trichodesmium*: a computer-model prediction. In: Marine Pelagic Cyanobacteria: *Trichodesmium* and Other Diazotrophs. Springer, pp. 239–248.

Kuhlisch, C., Althammer, J., Sazhin, A.F., Jakobsen, H.H., Nejstgaard, J.C., Pohnert, G., 2020. Metabolomics-derived marker metabolites to characterize *phaeocystis pouchetii* physiology in natural plankton communities. Sci. Rep. 10 (1), 20444.

Li, J., Li, Y., Bi, S., Xu, J., Guo, F., Lyu, H., Dong, X., Cai, X., 2022. Utilization of GOCI data to evaluate the diurnal vertical migration of *microcystis aeruginosa* and the underlying driving factors. J. Environ. Manag. 310, 114734.

McCloskey, G., Baheerathan, R., Dougall, C., Ellis, R., Bennett, F., Waters, D., Darr, S., Fentie, B., Hateley, L., Askildsen, M., 2021a. Modelled estimates of dissolved inorganic nitrogen exported to the Great Barrier Reef lagoon. Mar. Pollut. Bull. 171, 112655.

McCloskey, G., Baheerathan, R., Dougall, C., Ellis, R., Bennett, F., Waters, D., Darr, S., Fentie, B., Hateley, L., Askildsen, M., 2021b. Modelled estimates of fine sediment and particulate nutrients delivered from the Great Barrier Reef catchments. Marine pollution bulletin 165, 112163.

McCloskey, G., Waters, D., Baheerathan, R., Darr, S., Dougall, C., Ellis, R., Fentie, B., Hateley, L., 2017. Modelling pollutant load changes due to improved management practices in the Great Barrier Reef catchments: updated methodology and results – Technical Report for Reef Report Card 2014. Queensland Department of Natural Resources and Mines, Brisbane, Queensland.

McNown, J.S., Malaika, J., 1950. Effects of particle shape on settling velocity at low Reynolds numbers. EOS Trans. Am. Geophys. Union 31 (1), 74–82.

Moran, D., Robson, B., Gruber, R., Waterhouse, J., Logan, M., Petus, C., Lewis, S., Tracey, D., James, C., Mellors, J., Bove, U., Davidson, J., Glasson, K., Jaworski, S., Lefevre, C., Macadam, A., Shanahan, M., Vasile, R., Zagorskis, I., Shellberg, J., 2022. Marine Monitoring Program: Annual Report for Inshore Water Quality Monitoring 2020-21, booksubtitle=Report for the Great Barrier Reef Marine Park Authority. Great Barrier Reef Marine Park Authority, Townsville.

Oliver, R.L., 1994. Floating and sinking in gas-vacuolate cyanobacteria1. J. Phycol. 30 (2), 161–173.

Oliver, R.L., Hamilton, D.P., Brookes, J.D., Ganf, G.G., 2012. Physiology, blooms and prediction of planktonic cyanobacteria. In: Ecology of Cyanobacteria II: Their Diversity in Space and Time. Springer, pp. 155–194.

Post, A., Dedej, Z., Gottlieb, R., Li, H., Thomas, D., El-Absawi, M., El-Naggar, A., El-Gharabawi, M., Sommer, U., 2002. Spatial and temporal distribution of Trichodesmium spp. in the stratified Gulf of Aqaba, Red Sea. Mar. Ecol. Prog. Ser. 239, 241–250.

Qiu, J., Su, T., Wang, X., Jiang, L., Shang, Y., Jin, P., Xu, J., Fan, J., Li, W., Li, F., 2022. Comparative study of the physiological responses of *skeletonema costatum* and *thalassiosira weissflogii* to initial pCO_2 in batch cultures, with special reference to bloom dynamics. Mar. Environ. Res. 175, 105581.

Reynolds, C., Walsby, A., 1975. Water-blooms. Biol. Rev. 50 (4), 437–481.

Robson, B., Andrewartha, J., Baird, M., Herzfeld, M., Jones, E., Margvelashvili, N., Mongin, M., Rizwi, F., Skerratt, J., Wild-Allen, K., 2017. Evaluating the eReefs Great Barrier Reef marine model against observed emergent properties. In: MODSIM2017, 22nd International Congress on Modelling and Simulation. Modelling and Simulatio N Society of Australia and New Zealand. pp. 1976–1982.

Robson, B.J., Baird, M., Wild-Allen, K., 2013. A physiological model for the marine cyanobacteria, *trichodesmium*. In: MODSIM2013, 20th International Congress on Modelling and Simulation. Modelling and Simulation Society of Australia and New Zealand, ISBN (978-0).

Robson, B.J., Skerratt, J., Baird, M.E., Davies, C., Herzfeld, M., Jones, E.M., Mongin, M., Richardson, A.J., Rizwi, F., Wild-Allen, K., et al., 2020. Enhanced assessment of the ereefs biogeochemical model for the Great Barrier Reef using the Concept/State/Process/System model evaluation framework. Environ. Model. Softw. 129, 104707.

Romans, K.M., Carpenter, E.J., Bergman, B., 1994. Buoyancy regulation in the colonial diazotrophic cyanobacterium *trichodesmium tenue*: Ultrastructure and storage of carbohydrate, polyphosphate, and nitrogen 1. J. Phycol. 30 (6), 935–942.

Ryderheim, F., Hansen, P.J., Kiørboe, T., 2022. Predator field and colony morphology determine the defensive benefit of colony formation in marine phytoplankton. Front. Mar. Sci. 9, 829419.

Skerratt, J., Mongin, M., Baird, M., Wild-Allen, K., Robson, B., Schaffelke, B., Davies, C., Richardson, A., Margvelashvili, N., Soja-Wozniak, M., et al., 2019. Simulated nutrient and plankton dynamics in the Great Barrier Reef (2011–2016). J. Mar. Syst. 192, 51–74.

Stokes, G., 1850. On the effect of internal friction of fluids on the motion of pendulums. Trans. Cambr. phi1. S0c 9 (8), 106.

Subramaniam, A., Carpenter, E.J., Karentz, D., Falkowski, P.G., 1999. Bio-optical properties of the marine diazotrophic cyanobacteria *trichodesmium* spp. I. Absorption and photosynthetic action spectra. Limnol. Oceanogr. 44 (3), 608–617.

Ueno, Y., Aikawa, S., Kondo, A., Akimoto, S., 2016. Energy transfer in cyanobacteria and red algae: confirmation of spillover in intact megacomplexes of phycobilisome and both photosystems. J. Phys. Chem. Lett. 7 (18), 3567–3571.

Villareal, T., Carpenter, E., 2003. Buoyancy regulation and the potential for vertical migration in the oceanic cyanobacterium *trichodesmium*. Microb. Ecol. 45 (1), 1–10.

Walsby, A.E., 1969. The permeability of blue-green algal gas-vacuole membranes to gas. Proc. R. Soc. Lond. Ser. B 173 (1031), 235–255.

Walsby, A., 1978. The properties and buoyancy-providing role of gas vacuoles in *trichodesmium ehrenberg*. Br. Phycol. J. 13 (2), 103–116.

Walsby, A., 1992. The gas vesicles and buoyancy of *trichodesmium*. In: Marine pelagic cyanobacteria: Trichodesmium and other diazotrophs. Springer, pp. 141–161.

Walsby, A.E., Holland, D.P., 2006. Sinking velocities of phytoplankton measured on a stable density gradient by laser scanning. J. R. Soc. Interface 3 (8), 429–439.

Wei, K., Amano, Y., Machida, M., 2021. The effect of pH and light on the colony formation and buoyancy of *microcystis aeruginosa* UTEX-2061. Water Air Soil Pollut. 232, 1–11.

White, A., Karl, D., Björkman, K., Beversdorf, L., Letelier, R., et al., 2010. Production of organic matter by *trichodesmium* IMS101 as a function of phosphorus source. Limnol. Oceanogr. 55 (4), 1755.

White, A.E., Spitz, Y.H., Letelier, R.M., 2006. Modeling carbohydrate ballasting by *trichodesmium* spp.. Mar. Ecol. Prog. Ser. 323, 35–45.

Willmott, C.J., Ackleson, S.G., Davis, R.E., Feddema, J.J., Klink, K.M., Legates, D.R., O'donnell, J., Rowe, C.M., 1985. Statistics for the evaluation and comparison of models. J. Geophys. Res.: Oceans 90 (C5), 8995–9005.

Wu, K., Tang, S., Wu, X., Zhu, J., Song, J., Zhong, Y., Zhou, J., Cai, Z., 2023. Colony formation of *phaeocystis globosa*: A case study of evolutionary strategy for competitive adaptation. Mar. Pollut. Bull. 186, 114453.

Xu, G., Zhang, Y., Yang, T., Wu, H., Lorke, A., Pan, M., Xiao, B., Wu, X., 2023. Effect of light-mediated variations of colony morphology on the buoyancy regulation of *microcystis* colonies. Water Res. 235, 119839.

Yu, Q., Liu, Z., Chen, Y., Zhu, D., Li, N., 2018. Modelling the impact of hydrodynamic turbulence on the competition between *microcystis* and *chlorella* for light. Ecol. Model. 370, 50–58.